Detection of Magnetic Nanoparticles in Tissue Using Magneto-Motive DP-OCT

Junghwan Oh

University of Texas M.D. Anderson Cancer Center, Houston, Texas, USA

Ho Lee

School of Mechanical Engineering, Kyungpook National University, Daegu, Korea

Jeehyun Kim*

Computer Engineering Department, Kyungpook National University, Daegu, Korea

We demonstrate the capability of differential-phase optical coherence tomography (DP-OCT) to detect superparamagnetic iron oxide (SPIO) nanoparticles taken up by liver parenchymeal macrophages (Kupffer cells). We apply an external time-varying high-intensity focused magnetic field. Our experiments demonstrate a novel diagnostic modality to detect macrophages that have taken up SPIO nanoparticles. Magnetic force acting on the nanoparticles was varied by applying a sinusoidal current to a solenoid containing a conical iron core that substantially increased and focused the magnetic field strength (B_{max} = 2 Tesla). ApoE$^{/-}$ mice were sacrificed 2 days post intravenous injections of different SPIO doses (1.0, and 0.1 mmol *Fe*/kg body weight). Livers of ApoE$^{/-}$ mice with and without injection of SPIO nanoparticles were investigated using DP-OCT, which detects tissue movement with nanometer resolution. Frequency response of iron-laden liver movement was twice the stimulus frequency. Movement was not observed in livers of control mice. Results of our experiments indicate DP-OCT is a candidate methodology to detect tissue based macrophages containing SPIO nanoparticles excited by an external focused magnetic field.

OCIS codes : 170.0170, 030.0030, 110.0110, 140.0140

I. INTRODUCTION

Optical coherence tomography (OCT) [1] is a rapidly emerging imaging modality demonstrating improved resolution (< 10 µm) over competing techniques such as ultrasound, magnetic resonance imaging (MRI), and multi-sliced computed tomography (CT). Differential-phase optical coherence tomography (DP-OCT) is capable of high path length sensitivity and is able to detect a 1 µm optical path length change ($\triangle p$) between discrete reflecting surfaces [2]. DP-OCT has been used to measure displacement of nanometer-scale changes corresponding to neuron activity [3], electro kinetic response of cartilage [4], photo-thermal response of tissue [5], and phase contrast imaging of cells [6].

Use of superparamagnetic iron oxide (SPIO) nano-particles as a tissue specific contrast agent provides a variety of potential applications in biology and medicine. A common application of SPIO nanoparticles is as a liver-specific MRI contrast agent to detect macrophages and other phagocytic cells in the reticuloendothelial system (RES) [7]. Macrophages in cardiovascular disease are considered an important marker of vulnerable fibrous caps and a subsequent inflammatory mediated plaque rupture [8]. Detection of macrophages may also have utility for diagnosis of early stage cancer due to phagocytosis of malignant cells [9]. In the current study we hypothesized that tissue based macrophages could be detected by placing engulfed SPIO nanoparticles in motion with an externally applied oscillating magnetic field. Since the ensuing motion of SPIO nanoparticles was anticipated to be on the order of nanometers, we used DP-OCT to detect tissue surface displacement in response to an applied magnetic field. We tested this hypothesis in ApoE$^{/-}$ mice since tissue based macro-phages in the liver, Kupffer cells, were found previously to take up SPIO nanoparticles in a robust fashion [7].

II. MATERIALS AND METHODS

2.1 Superparamagnetic iron oxide (SPIO) nanoparticles

SPIO nanoparticles are tissue-specific MRI contrast agents approved in 1996 by the United States Food and Drug Administration (FDA) for human hepatic disease to enhance image contrast. SPIO nanoparticles are also known as Ferumoxides or AMI-25 and their trade name is Feridex I.V. (USA) and Endorem (EU) [10]. Commercial magnetic nanoparticles can be classified by the overall size and surface coating. The mean core diameter of SPIO nanoparticles is 20 nm and total aggregation diameter is about 100 nm [11]. SPIO nanoparticles consist of nonstoichiometric magnetite crystalline cores, iron, and a dextran T-10 coating that is used to prevent aggregation and provide stabilization in the liver. Following injection of SPIO nanoparticles into rats, 80% of injected nanoparticles accumulate in tissue-based macrophages (Kupffer cells) in the liver due to the relatively short blood half life [7]. Uptake of SPIO nanoparticles by macrophage cells is directly dependent on concentration of intravenous (IV) injection, blood half life, and core size inside nanoparticles [12].

2.2 Magnetic force on superparamagnetic iron oxide (SPIO) nanoparticles

Magnetic force acting on SPIO nanoparticles becomes:

$$\mathbf{F} = -\nabla U = \nabla(\frac{\chi_s V}{2u_0}|\mathbf{B}|^2) = \chi_s V \nabla(\frac{|\mathbf{B}|^2}{2u_0}) . \tag{1}$$

We assume a sinusoidal magnetic flux density that is directed principally along the z-direction. Hence, we write $\vec{B}(x, y, z; t) = \sin(2\pi f_n t)B_z(z)\hat{k}$ and the magnetic force $\mathbf{F_m}$ acting on nanoparticles,

$$\mathbf{F_m} = \frac{\chi_s V_s}{2\mu_0}[1 - \cos(4\pi f_n t)]\mathbf{B}_z(z)\frac{\partial \mathbf{B}_z}{\partial z} \tag{2}$$

Where f_n is the modulation frequency of the applied sinusoidal magnetic field. The total force acting on nanoparticles in the z-direction is written

$$\sum \mathbf{F}_z = m\frac{\partial^2 z(t)}{\partial t^2} = \mathbf{F_m} - kz_{np}(t) - r\frac{\partial z_{np}}{\partial t} \tag{3}$$

Where $kz_{np}(\text{t})$ is an elastic restoring force, and $r\frac{\partial z_{np}}{\partial t}$ is a drag force that accounts for the viscous properties of the local tissue environment. The negative sign of viscous drag and restoring forces indicates that these forces are in opposite direction to nanoparticle move-

ment, $z_{np}(\text{t})$. We can write equations of motion by dividing by the mass, m.

$$\frac{\partial^2 z_{np}(t)}{\partial t^2} + \frac{r}{m}\frac{\partial z_{np}}{\partial t} + \frac{kz_{np}(t)}{m} = \frac{\chi_s V_s}{2m\mu_0}[1 - \cos(4\pi f_n t)]B_z(z)\frac{\partial B_z}{\partial z} \tag{4}$$

Equation (4) can be rewritten using the first terms in the Maclaurin series for the magnetic field and its gradient,

$$\frac{\partial^2 z_{np}(t)}{\partial t^2} + \frac{r}{m}\frac{\partial z_{np}}{\partial t} + \frac{kz_{np}(t)}{m} \cong \frac{\chi_s V_s}{2m\mu_0}[1 - \cos(4\pi f_n t)]\mathbf{B}_z(0)\frac{\partial \mathbf{B}_z(0)}{\partial z} \tag{5}$$

Letting $a = \frac{x_s V_s}{2m\mu_0}\mathbf{B}_z(0)\frac{\partial \mathbf{B}_z(0)}{\partial z}$, $\omega_B = 4\pi f_n$, $k/m = \omega_0^2$, and $r/m = \gamma$, the second order differential equation (5) may be written

$$\frac{\partial^2 z_{np}(t)}{\partial t^2} + \gamma\frac{\partial z_{np}}{\partial t} + \omega_0^2 z_{np}(t) = a[1 - \cos(\omega_B t)] , \tag{6}$$

The Laplace transform may be used to solve the second order differential equation (6). We assume zero initial displacements and velocity to find;

$$s^2 Z_{np}(s) + \frac{r}{m}sZ_{np}(s) + \frac{k}{m}Z_{np}(s) = \frac{a}{s} - \frac{as}{(s^2 + \omega_B^2)}$$

$$Z_{np}(s) = \frac{\frac{a}{s} - \frac{as}{(s^2 + \omega_B^2)}}{(s^2 + \gamma s + \omega_0^2)} = a\left(\frac{1}{(s^2 + \gamma s + \omega_0^2)s} - \frac{s}{(s^2 + \gamma s + \omega_0^2)}\right) \tag{7}$$

If $4\omega_0^2 - \gamma^2 > 0$, we can write nanoparticle movement $(z_{np}(\text{t}))$ by computing the sum of transforms.

$$z_{np}(t) = \frac{a\left[\begin{matrix}-\gamma\omega_B\omega_0^2\sin(\omega_B t) + (\gamma^2\omega_B^2 - 2\omega_B^2\omega_0^2 + \omega_B^4 + \omega_0^4) - \omega_0^4\cos(\omega_B t) + (\omega_B^2\omega_0^2)\cos(\omega_B t) + \\ \exp(-\frac{1}{2}\gamma t)\left(\frac{-\omega_B^2(\gamma^2 + \omega_B^2 - \omega_0^2)\cos(\frac{1}{2}t(4\omega_0^2 - \gamma^2)^{\frac{1}{2}}) - }{\omega_B^2\gamma(-3\omega_0^2 + \omega_B^2 + \gamma^2)\sin(\frac{1}{2}t(4\omega_0^2 - \gamma^2)^{\frac{1}{2}})}\right)}{(4\omega_0^2 - \gamma^2)^{\frac{1}{2}}}\end{matrix}\right]}{(\omega_0^2(\gamma^2\omega_B^2 - 2\omega_B^2\omega_0^2 + \omega_B^4 + \omega_0^4))} \tag{8}$$

We find the displacement $(z_{np}(\text{t}))$ of nanoparticles by using an inverse Laplace transform; the solution includes transient and steady state terms. The initial motion of magnetic nanoparticles is driven by a constant magnetic force and displays a damped transient motion before steady state motion dominates at twice the modulation frequency of the applied sinusoidal magnetic field. Motion of the nanoparticles at double the modulation frequency originates from the magnetic force being proportional to the product of magnetic

flux density and the gradient (equation (4)).

2.3 Magnetic field generator

The magnetic field generator consists of a solenoid (Ledex 6EC, Saia-Burgess Inc., USA), a function generator (HP 33120A, Hewlett Packard Inc., USA), a current amplifier and a power supply. The FEM simulation demonstrated that an iron core positioned along the centerline of the solenoid dramatically increased magnetic flux density at the target specimen. Magnetic field distributions from the FEM simulation showed the maximal and principal direction of the magnetic field strength was along the z-direction. The conical iron core provided focusing and substantially increased the magnetic field strength. Magnetic flux density at the sample with an iron core positioned in the solenoid was about ten times greater than that without a core.

2.4 Animal model and histology

Liver tissues from 12 week old ApoE$^{-/-}$ high fat fed mice were utilized in this study because they contain tissue based macrophages cells. All experimental procedures were performed in accordance with protocols approved by the University of Texas Institutional Animal Care and Use Committee. The mice were injected via the jugular vein with either Feridex I.V.

(Ferumoxides injectable solutions; Berelex Laboratories, USA) for IV administration (1.0, 0.1 mmol Fe/kg body weight) or saline, and sacrificed 2 days post intravenous injection. The mice were euthanized with a lethal dose of Ketamine and Xylazine. After euthanizing, abdominal incisions were made to remove the entire liver from the mouse. Physical thickness of the liver samples was fixed at 1 mm and 0.5 cm x 0.5 cm in lateral dimensions. After completion of DP-OCT measurements, the mouse livers were embedded in 10% formalin acid and processed for histology. Sections 5 μm thick were cut and stained with Prussian blue to identify iron deposition in liver Kupffer cells. To verify SPIO uptake by macrophage cells from histology slides, Image Pro Plus (Mediacynernetics Inc., USA) software was used to measure the total area of liver and accumulated area of SPIO aggregation that is Prussian blue positive.

2.5 DP-OCT measurements

Figure 1 shows a schematic diagram of a fiber-based dual channel differential-phase optical coherence tomography (DP-OCT) system (a), and sample path configuration with magnetic field generator (b). The dual-channel Michelson interferometer was used to measure differential phase between light backscattered from a glass reference surface and liver surface when applying a sinusoidal focused magnetic field. Optical path length
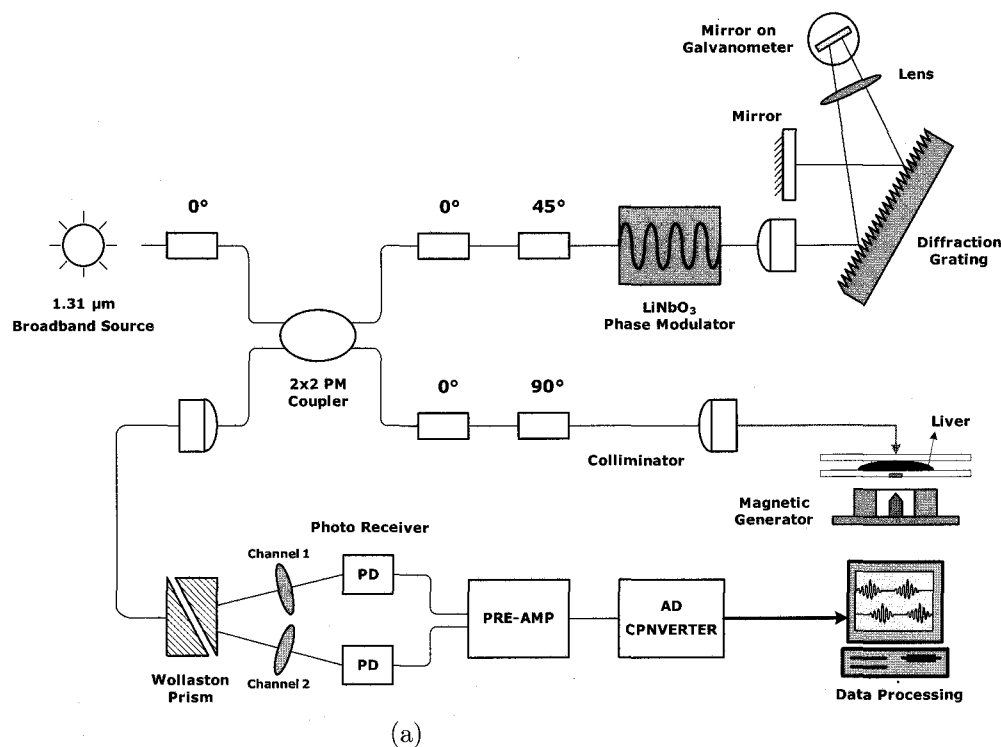

(a)

FIG. 1. Schematic diagram of a differential phase optical coherence tomography (DP-OCT) system combined with a magnetic field generator:

change measured in this study corresponds to tissue surface displacement $z_s(t)$ in response to a high-strength magnetic field applied to iron-laden tissue and can be calculated from the differential phase ($\triangle\varphi$) and central wavelength of source light ($\lambda_0 = 1310$ nm),

$$z_s(t) = \frac{\lambda_0}{4\pi}(\varphi_{ch1} - \varphi_{ch2}) = \frac{\lambda_0}{4\pi}\Delta\varphi \qquad (9)$$

The two signals recorded from Channel 1 and 2 by the DP-OCT system were used to measure tissue surface displacement $z_s(t)$ due to movement of the SPIO nanoparticles.

III. RESULTS

Differential-phase OCT (DP-OCT) measurements were performed on isolated liver specimens taken from ApoE$^{/-}$ mice administered different SPIO doses (1.0, and 0.1 mmol Fe/kg body weight) and saline control samples. Figure 3 demonstrates measurements of tissue surface displacement ($z_s(t)$) in liver specimens at different SPIO doses (1.0, and 0.1 mmol Fe/kg body weight) and saline control samples, in response to application of a sinusoidal varying high-intensity focused magnetic field. Measurement of tissue surface displacement ($z_s(t)$) was begun after transient response

was negligible and steady state motion persisted. Figure 2 (a) shows a magnetic field input ($f_n = 2$ Hz), peak-to-peak voltage ($V_{pp} = 4$) over a 1 second time period. Maximum magnetic flux density was 0.47 Tesla and maximal tissue surface displacement ($\triangle z_s(t)$) was 2,273 nm in the 1.0 mmol Fe/kg iron-laden liver. Compared to high dose specimens, 0.1 mmol Fe/kg iron-laden liver showed a maximum tissue surface displacement ($\triangle z_s(t)$) of 127 nm with additive noise visible in recorded signals. Frequency response (4 Hz) of iron-laden livers (figure 2 (b), (c)) was exactly twice the modulation frequency (2 Hz) as noted earlier. No significant tissue surface displacement ($z_s(t)$) was observed in saline control liver specimens (figure 3 (d)).

SPIO nanoparticle movement in iron laden livers (0.1, and 1.0 mmol Fe/kg) was used to observe quantitatively the relationship between tissue surface displacement ($z_s(t)$) versus different applied magnetic field strengths (figure 3 (a)). Solenoid input frequency in this experiment was 2 Hz with amplitude ranging from 2 to 8 V_{pp}. Figure 3 (b) shows magnetic flux density at the same voltages as in figure 3 (a). Magnitude of tissue surface displacement ($z_s(t)$) of iron-laden liver specimens depended directly on SPIO dose and strength of the external magnetic field. Tissue surface displacement ($z_s(t)$) at high frequency modulation (over 100 Hz) was negligible.

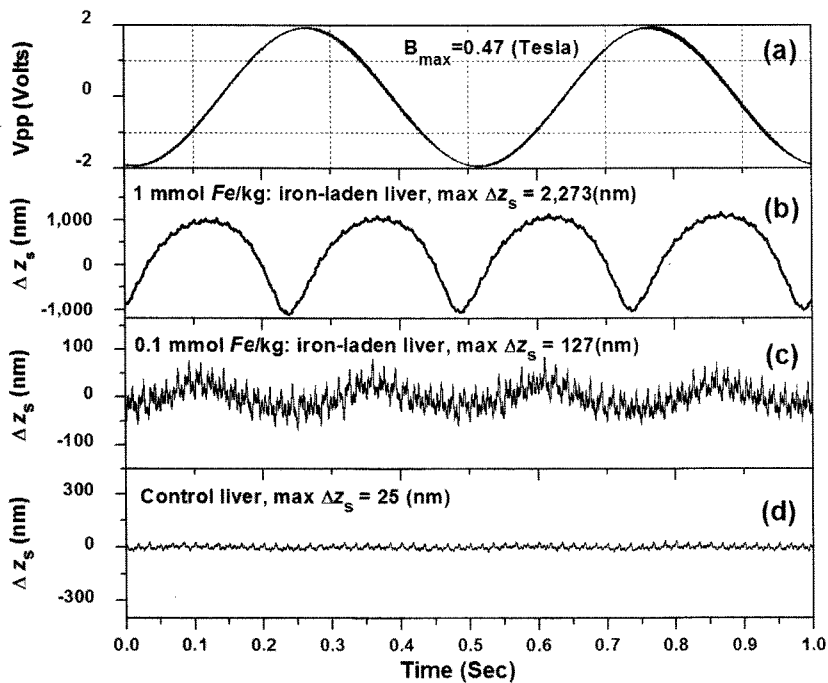Maximum tissue surface displacement ($\triangle z_s(t)$) in

FIG. 2. Maximum tissue surface displacement ($\triangle z_s$) in livers with different SPIO doses (1.0, 0.1 mmol Fe/kg and saline control) using focused magnetic field excitation (2 Hz, 4 V_{pp}) (a). Tissue surface displacement ($\triangle z_s$) in specimens with doses 1.0 mmol Fe/kg SPIO (b), 0.1 mmol Fe/kg SPIO (c), and a saline control liver (d). The applied magnetic flux density is $B_{max} = 0.47$ Tesla at the liver specimen.
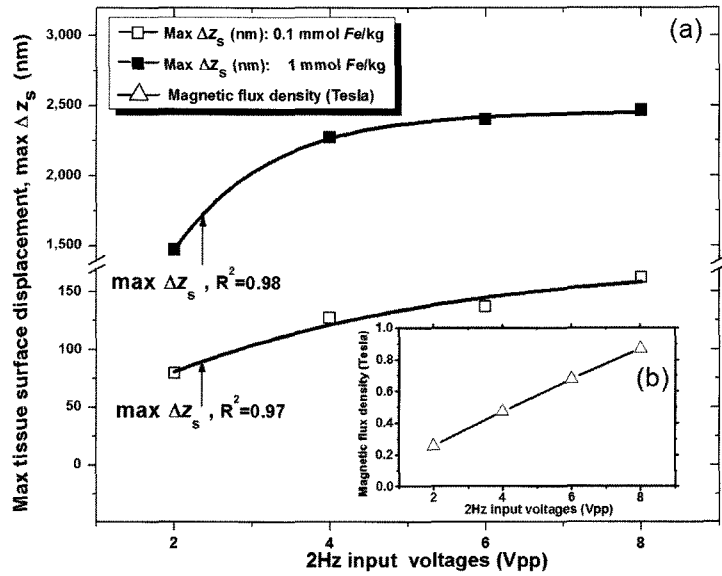
FIG. 3. Maximum tissue surface displacement ($\triangle z_s$) in iron-laden liver specimens due to nanoparticle movement in response to a focused magnetic field for mice injected with various SPIO doses (1.0 and 0.1 mmol Fe/kg). The input frequency is 2 Hz with applied voltage ranging from 2 to 8 V_{pp} (a) and magnetic field strength at each input voltage (b).
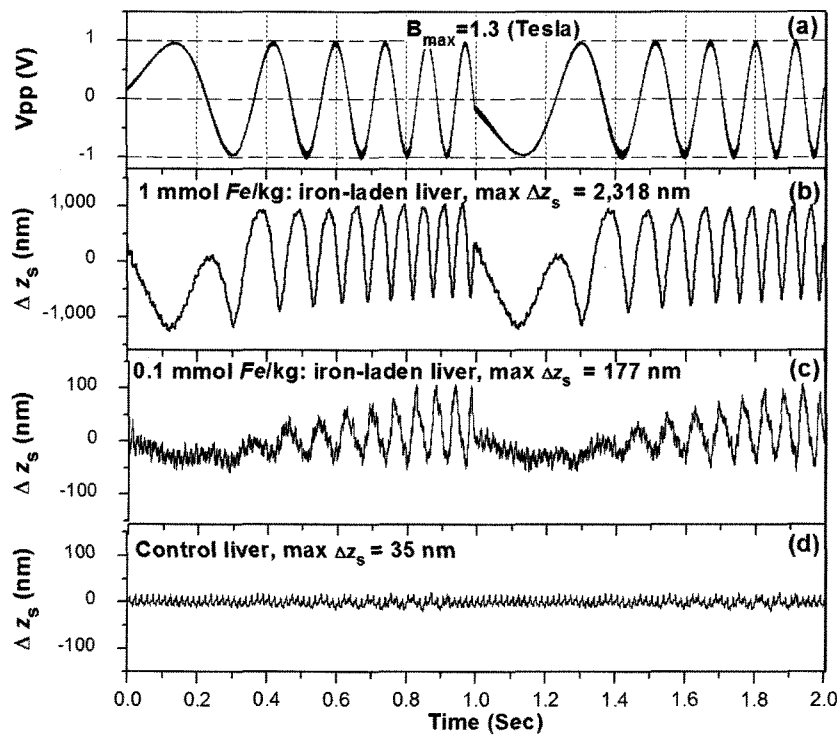

FIG. 4. Maximum tissue surface displacement ($\triangle z_s$) in iron-laden liver specimens due to nanoparticle movement in response to a focused magnetic field with a swept frequency (1~10 Hz) input for mice injected with various SPIO doses (1.0 and 0.1 mmol Fe/kg). (a). Tissue surface displacement ($\triangle z_s$) at 1.0 mmol Fe/kg SPIOdose (b), 0.1 mmol Fe/kg SPIO dose (c), and a saline control liver (d). The applied focused magnetic flux density is 1.3 Tesla at the specimen.

iron-laden liver specimens (0.1 and 1.0 mmol Fe/kg) can be measured using a swept input frequency. Figure 4 (a) shows the magnetic field input with a swept frequency increasing from 1 to 10 Hz over a 2 second time-period. Maximum tissue surface displacement ($\triangle z_s(t)$) was 2,318 nm in a high dose liver (1.0 mmol Fe/kg) and 177 nm in a low dose specimen (0.1 mmol Fe/kg), and magnetic field intensity was 1.3 Tesla.
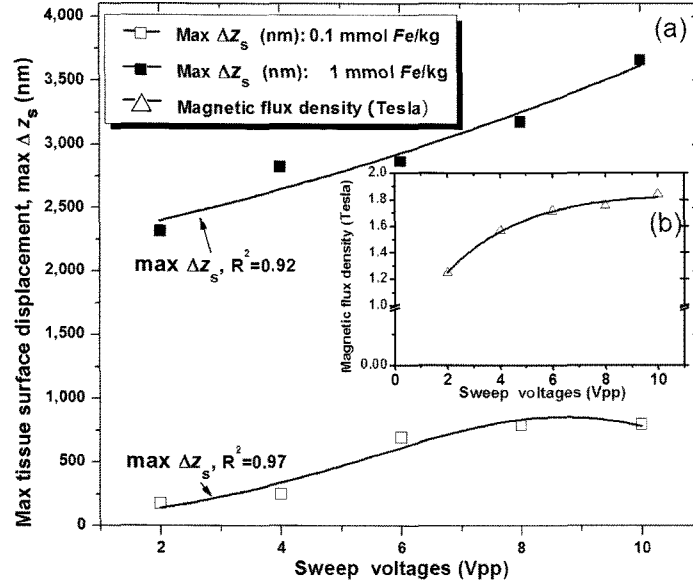
FIG. 5. Maximum tissue surface displacement ($\triangle z_s$) in iron-laden liver specimens due to nanoparticle movement in response to a focused magnetic field with a swept frequency ($1 \sim 10$ Hz) input for mice injected with various SPIO doses (1.0 and 0.1 mmol Fe/kg). Input swept frequency ranged from $1 \sim 10$ Hz over 2 seconds with input voltages increasing from 2 to 10 V_{pp} (a) and magnetic field strength at each input voltage (b).
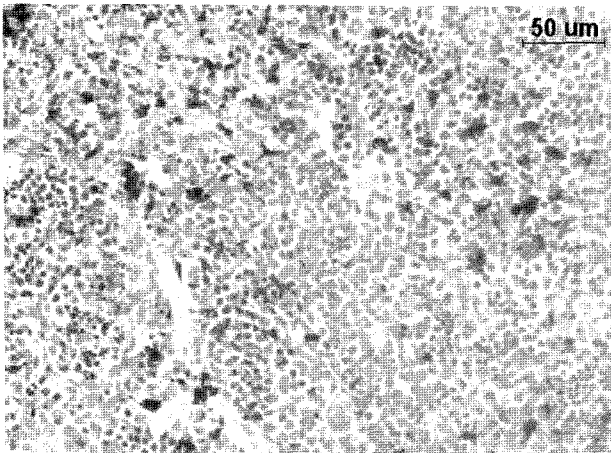

FIG. 6. Histological cross-section of iron laden liver specimen with Prussian blue stain. A high concentration of iron is observed (magnification: 20 X). Blue colored regions are iron nanoparticles engulfed by liver based macrophage Kupffer cells.

Frequency response of the force acting on iron-laden liver specimens is exactly twice the externally applied modulation frequency in figure 4 (b) and (c). No significant tissue surface displacement was observed in saline control liver specimens shown in figure 5 (d).

Figure 5 illustrates maximum tissue surface displacement ($\triangle z_s(t)$) in a iron-laden mouse liver to observe quantitatively the relationship between magnetic response in tissue versus different applied magnetic field strengths with a swept-source frequency ranging from

1-10 Hz over a 2 second time-period. Maximum tissue surface displacement ($\triangle z_s(t)$) was larger when input voltage was gradually increased from 2 to 10 V_{pp} during a frequency sweep. Corresponding magnetic field strength at these voltages was 1.24 (2 V_{pp}), 1.58 (4 V_{pp}), 1.71 (6 V_{pp}), 1.75 (8 V_{pp}) and 1.84 Tesla (10 V_{pp}), respectively. For a given frequency sweep, maximum tissue surface displacement ($\triangle z_s(t)$) for 0.1 and 1.0 mmol Fe/kg iron-laden liver specimens was 3700 nm and 750 nm, respectively, at 10 V_{pp} and magnetic field strength of 1.84 Tesla.

SPIO nanoparticles are identified in histological sections as blue granules from the Prussian blue stain of iron laden mouse livers (figure 6). Compared to controls, iron laden specimens show significant discrete granular iron accumulations evenly distributed in observed areas. Although intracellular iron was also observed in control specimens, this natural iron was uniform and homogeneous rather than appearing in discrete granular shapes. Total SPIO iron area was 12% of the histology image as calculated by Image-Pro PLUS 5.1 software.

IV. DISCUSSION

In this study, we have demonstrated a novel quantitative diagnostic imaging modality, by using DP-OCT and a high-intensity focused magnetic field, to specifically detect tissue based macrophages that have taken up iron nanoparticles. Magnetic force acting on the

nanoparticles was varied by applying a sinusoidal current (2 Hz and a swept frequency (1~10 Hz)) to a solenoid containing a conical iron core that substantially increased and focused the magnetic field strength (B_{max} = 2 Tesla). Frequency response of tissue surface displacement from iron-laden macrophages was exactly twice the exciting frequency of the input magnetic field in figure (3) and (5). At excitation frequencies over 100 Hz, tissue surface displacement ($z_s(t)$) was too small to measure and evaluate because SPIO nanoparticles and surrounding material did not respond to the applied magnetic field. Our results suggest that DP-OCT may allow detection of liver-based macrophages at relatively low dose of SPIO nanoparticles (0.1 mmol Fe/kg body weight) with nanometer resolution.

SPIO nanoparticles, composed of dextran T-10 (Ferumoxides) coated iron oxide, were some of the first materials investigated as MRI contrast agents [14], and more recently used to image focal hepatic lesions in patients using MRI [15]. It is notable that SPIO nanoparticles have been explored for other imaging applications such as detection of malignant lymph nodes [16], brain tumors [17] and bone marrow [18] using contrast enhanced MRI. These particles have also been investigated for use to identify early stages of atherosclerotic vulnerable plaque to image macrophage cells that selectively take up these nanoparticles [19, 20]. More recently, SPIO agent applications have been extended to magnetic separation and sorting of biological molecules [21], targeted drug delivery [22], and magnetic therapeutic hyperthermia using a high frequency magnetic field [23].

Preliminary experiments to quantify macrophages in coronary arteries of patients were performed [24] using intravascular OCT. However, lack of specificity of this approach is noted; for instance, darker OCT images with 10 μm resolution correlated with macrophage presence in histology, but could not rule out contributions from other tissue components. Use of conventional OCT to measure macrophage density in the plaque wall and thereby evaluate macrophage content *in vivo* may be problematic due to confounding contributions from other tissue components. Magneto-motive OCT was demonstrated to enhance image contrast of macrophages *in vivo* in a tadpole [25] by imaging optical scattering changes in the specimens; however, in this work, the magnetic field strength (B_{max} = 0.06 Tesla) was significantly lower than in our experiment (B_{max} = 1.84 Tesla) and it did not a provide quantitative phase-based measurement of displacement in real heterogeneous tissue macrophages. In addition, fringe intensity modulation due to nanoparticle movement utilized in this study may not offer optimal contrast enhancement to identify macrophages with high sensitivity.

Measured tissue surface displacement ($z_s(t)$, equation (8)) and computed nanoparticle movement ($z_{np}(t)$, equation (9)) are related but distinct physical quantities. Amplitude of tissue surface displacement will be increasingly less than nanoparticle movement while nanoparticles are positioned deeper in the tissue. In the limit that nanoparticles are positioned at the tissue surface, tissue surface displacement ($z_s(t)$) is equal to nanoparticle movement ($z_{np}(t)$). Quantitative interpretation of tissue surface displacement ($z_s(t)$) in specimens containing SPIO nanoparticles will require further study and necessitate a mathematical model incorporating viscoelastic tissue properties. A mathematical model incorporating the viscoelastic properties of tissue will allow quantitative analysis of tissue displacement for a given movement of nanoparticles.

Nanoparticle movement by an externally applied magnetic field consists of two motions from equation (8); transient and steady state. After transient response, physical displacement approaches a steady state response, which resembles the input sinusoidal signal and was measured in this study.

$$z_{np(stead)}(t) = a\left(\frac{1}{\omega_0^2} + \frac{\left(\omega_B^2 - \omega_0^2\right)\cos(\omega_B t)}{(\gamma^2 \omega_B^2 - 2\omega_B^2 \omega_0^2 + \omega_B^4 + \omega_0^4)} \right.$$
$$\left. - \frac{\gamma \omega_B \sin(\omega_B t)}{(\gamma^2 \omega_B^2 - 2\omega_B^2 \omega_0^2 + \omega_B^4 + \omega_0^4)} \right) \qquad (10)$$

Amplitude of nanoparticle movement in steady state ($z_{np(steady)}(t)$, equation (10)) depends on the magnetic field and its gradient from, $a = \frac{x_s V_s}{2m\mu_0} B_z(0) \frac{\partial B_z(0)}{\partial z}$. In equation (10), the maximum amplitude of nanoparticle displacement in steady state measured in our study occurs when $\omega_B^2 = \omega_0^2 - \frac{\gamma^2}{2}$. Alternatively when $\omega_0 \gg \omega_B$, amplitude of nanoparticle movement diminishes to zero. Variation of amplitude in tissue surface displacement ($z_s(t)$) by applying swept frequency (figure 5 (b) and (c)) may be associated with spatial variations of viscoelastic tissue properties (γ, ω_0) in different specimens and further experimental studies and mathematical simulations will be required to evaluate spatial variation of γ and ω_0.

In conclusion, frequency response of tissue movement in response to an externally applied magnetic field was twice the stimulus frequency and is consistent with established magnetodynamic principles. Increasing the magnetic field strength increased surface displacement of liver specimens. In saline control liver specimens, no significant tissue surface displacement ($z_s(t)$) was observed in response to an externally applied magnetic field. Results of our experiments suggest DP-OCT in combination with an externally applied magnetic field

is a candidate methodology to identify tissue macro-phages containing SPIO nanoparticles.

*Corresponding author: jeehk@uci.edu

REFERENCES

[1] D. Huang, E. A. Swanson, C. P. Lin, J. S. Schuman, W. G. Stinson, W. Chang, M. R. Hee, T. Flotte, K. Gregory, C. A. Puliafito, and et al., "Optical coherence tomography," *Science*, vol. 254, pp. 1178-1181, 1991.

[2] D. P. Dave and T. E. Milner, "Optical low-coherence reflectometer for differential phase measurement," *Opt. Lett.*, vol. 25, pp. 227-229, 2000.

[3] T. Akkin, D. P. Dave, T. E. Milner, and H. G. Rylander, "Detection of neural activity using phase-sensitive optical low-coherence reflectometry," *Opt. Express.*, vol. 12, pp. 2377-2386, 2004.

[4] J. I. Youn, T. Akkin, and T. E. Milner, "Electrokinetic measurement of cartilage using differential phase optical coherence tomography," *Physiol. Meas.*, vol. 25, pp. 85-95, 2004.

[5] S. A. Telenkov, D. P. Dave, S. Sethuraman, T. Akkin, and T. E. Milner, "Differential phase optical coherence probe for depth-resolved detection of photothermal response in tissue," *Phys. Med. Biol.*, vol. 49, pp. 111-119, 2004.

[6] C. G. Rylander, D. P. Dave, T. Akkin, T. E. Milner, K. R. Diller, and A. J. Welch, "Quantitative phase-contrast imaging of cells with phase-sensitive optical coherence microscopy," *Opt. Lett.*, vol. 29, pp. 1509-1511, 2004.

[7] R. Weissleder, D. D. Stark, B. L. Engelstad, B. R. Bacon, C. C. Compton, D. L. White, P. Jacobs, and J. Lewis, "Superparamagnetic Iron-Oxide - Pharmaco-kinetics and Toxicity," *Am. J. Roentgenol.*, vol. 152, pp. 167-173, 1989.

[8] P. R. Moreno, E. Falk, I. F. Palacios, J. B. Newell, V. Fuster, and J. T. Fallon, "Macrophage Infiltration in Acute Coronary Syndromes - Implications for Plaque Rupture," *Circulation*, vol. 90, pp. 775-778, 1994.

[9] L. M. Coussens and Z. Werb, "Inflammation and cancer," *Nature*, vol. 420, pp. 860-867, 2002.

[10] C. W. Jung and P. Jacobs, "Physical and chemical pro-perties of superparamagnetic iron oxide MR contrast agents: ferumoxides, ferumoxtran, ferumoxsil," *Magn. Reson. Imaging.*, vol. 13, pp. 661-674, 1995.

[11] R. M. Weisskoff and S. Kiihne, "Mri Susceptometry - Image-Based Measurement of Absolute Susceptibility of Mr Contrast Agents and Human Blood," *Magnet. Reson. Med.*, vol. 24, pp. 375-383, 1992.

[12] Y. X. Wang, S. M. Hussain, and G. P. Krestin, "Super-paramagnetic iron oxide contrast agents: physicoche-mical characteristics and applications in MR imaging," *Eur. Radiol.*, vol. 11, pp. 2319-2331, 2001.

[13] J. F. Schenck, "Safety of strong, static magnetic fields," *J. Magn. Reson. Imaging.*, vol. 12, pp. 2-19, 2000.

[14] G. Marchal, P. Van Hecke, P. Demaerel, E. Decrop, C. Kennis, A. L. Baert, and E. van der Schueren, "Detection of liver metastases with superparamagnetic iron oxide in 15 patients: results of MR imaging at 1.5 T," *AJR. Am. J. Roentgenol.*, vol. 152, pp. 771-775, 1989.

[15] P. Reimer, N. Jahnke, M. Fiebich, W. Schima, F. Deckers, C. Marx, N. Holzknecht, and S. Saini, "Hepatic lesion detection and characterization: value of nonen-hanced MR imaging, superparamagnetic iron oxide-enhanced MR imaging, and spiral CT-ROC analysis," *Radiology*, vol. 217, pp. 152-158, 2000.

[16] K. Tsushima, A. Nishie, K. Yoshimitsu, A. Taketomi, and H. Honda, "Liver metastasis with apparent intra-tumoral superparamagnetic iron oxide uptake," *Eur. Radiol.*, vol. 15, pp. 2203-2204, 2005.

[17] R. L. Reddick, S. H. Zhang, and N. Maeda, "Athero-sclerosis in Mice Lacking Apo-E - Evaluation of Lesional Development and Progression," *Arterioscler. Thromb.*, vol. 14, pp. 839-839, 1994.

[18] W. Hundt, R. Petsch, T. Helmberger, and M. Reiser, "Effect of superparamagnetic iron oxide on bone marrow," *Eur. Radiol.*, vol. 10, pp. 1495-1500, 2000.

[19] P. Cherukuri, J. Wosik, J. D. Hazle, S. Litovsky, M. Madjid, W. Casscells, J. T. Willerson, and M. Naghavi, "Contrast-enhanced intravascular detection of vulnerable plaque using superparamagnetic iron oxide and a novel magnetic resonance imaging catheter.," *Am. J. Cardiol.*, vol. 90, pp. 23h-24h, 2002.

[20] S. A. Schmitz, S. E. Coupland, R. Gust, S. Winterhalter, S. Wagner, M. Kresse, W. Semmler, and K. J. Wolf, "Superparamagnetic iron oxide-enhanced MRI of athero-sclerotic plaques in Watanabe hereditable hyperlipidemic rabbits," *Invest. Radiol.*, vol. 35, pp. 460-471, 2000.

[21] T. M. Said, S. Grunewald, U. Paasch, M. Rasch, A. Agarwal, and H. J. Glander, "Effects of magnetic-activated cell sorting on sperm motility and cryosurvival rates," *Fertil. Steril.*, vol. 83, pp. 1442-1446, 2005.

[22] T. Neuberger, B. Schopf, H. Hofmann, M. Hofmann, and B. von Rechenberg, "Superparamagnetic nano-particles for biomedical applications: Possibilities and limitations of a new drug delivery system," *J. Magn. Magn. Mater.*, vol. 293, pp. 483-496, 2005.

[23] M. Chastellain, A. Petri, A. Gupta, K. V. Rao, and H. Hofmann, "Superparamagnetic silica-iron oxide nano-composites for application in hyperthermia," *Adv. Eng Mater.*, vol. 6, pp. 235-241, 2004.

[24] G. J. Tearney, H. Yabushita, S. L. Houser, H. T. Aretz, I. K. Jang, K. H. Schlendorf, C. R. Kauffman, M. Shishkov, E. F. Halpern, and B. E. Bouma, "Quan-tification of macrophage content in atherosclerotic plaques by optical coherence tomography," *Circulation*, vol. 107, pp. 113-119, 2003.

[25] A. L. Oldenburg, F. J. J. Toublan, K. S. Suslick, A. Wei, and S. A. Boppart, "Magnetomotive contrast for *in vivo* optical coherence tomography," *Opt. Express.*, vol. 13, pp. 6597-6614, 2005.